Geophysical Journal International

Geophys. J. Int. (2016) **206,** 395–407
Advance Access publication 2016 April 21
GJI Seismology

doi: 10.1093/gji/ggw159

Ellipticity of Rayleigh waves in basin and hard-rock sites in Northern Italy

Andrea Berbellini,[1,2] Andrea Morelli[1,2] and Ana M.G. Ferreira[3,4]

[1] *Dipartimento di Fisica e Astronomia, Alma Mater Studiorum - Università degli Studi di Bologna, Via Zamboni* 33, *I*-40126 *Bologna, Italy.*
E-mail: andrea.berbellini@ingv.it
[2] *Istituto Nazionale di Geofisica e Vulcanologia, Sezione di Bologna, Via Donato Creti* 12, *I*-40128 *Bologna, Italy*
[3] *Department of Earth Sciences, Faculty of Maths and Physical Sciences, University College London, WC1E6BT, United Kingdom*
[4] *CERIS, Instituto Superior Técnico, Universidade de Lisboa, Av. Rovisco Pais* 1, 1049-001 *Lisboa, Portugal*

Accepted 2016 April 19. Received 2016 March 21; in original form 2016 January 13

SUMMARY

We measure ellipticity of teleseismic Rayleigh waves at 95 seismic stations in Northern Italy, for wave period between 10 and 110 s, using an automatic technique and a large volume of high-quality seismic recordings from over 500 global earthquakes that occurred in 2008–2014. Northern Italy includes a wide range of crustal structures, from the wide and deep Po Plain sedimentary basin to outcropping sedimentary and crystalline rocks in the Northern Apennines and Alps. It thus provides an excellent case for studying the influence of shallow earth structure on polarization of surface waves. The ellipticity measurements show excellent spatial correlation with geological features in the region, such as high ellipticity associated with regions of low seismic velocity in the Po Plain and low ellipticity values in faster, hard rock regions in the Alps and Apennine mountains. Moreover, the observed ellipticity values also relate to the thickness of the basement, as highlighted by observed differences beneath the Alps and the Apennines. Comparison between observations and predicted ellipticity from a reference crustal model of the region show substantial fit, particularly for $T \sim 38$ s data. Discrepancy for shorter wave period suggests that slight modifications of the model are needed, and that the ellipticity measurements could help to better constrain the shallow crustal structure of the region. Predictions for the Po Plain are larger than the observations by a factor of four or more and transition from retrograde to prograde Rayleigh wave motion at the surface for periods of $T \sim 10$–13 s is predicted for seismic stations in the plain. Analysis of corresponding real data indicates a possible detection of teleseismic prograde particle motion, but the weak teleseismic earthquake signals are mixed with ambient noise signals at the predicted, short, transition periods. Detection of the period of polarity inversion from the joint analysis of earthquake and ambient noise ellipticity measurements may provide further, stringent, constraints on the structure of sedimentary basins.

Key words: Surface waves and free oscillations; Site effects; Seismic tomography; Wave propagation.

1 INTRODUCTION

Ellipticity of Rayleigh waves (also called H/V ratio) is defined as the ratio between the axes of the elliptically polarised particle motion, and is measured as the ratio between the displacement amplitude of horizontal and vertical components of the fundamental-mode wave train. In a flat layered medium or in a smooth, laterally heterogeneous medium, the H/V ratio depends only on the structure beneath the station, without any dependence on event distance, azimuth, depth or magnitude (e.g. Ferreira & Woodhouse 2007b). This represents a main advantage of the usage of this observable: using ellipticity, we can retrieve earth structure beneath each station without the need of a description of the structure between source and receiver. This feature is particularly relevant in areas with low or uneven data coverage. Ellipticity measurements do not require high seismicity rates in the study area because they can conveniently be performed on teleseismic records, so they can be carried out virtually anywhere. Ellipticity is more sensitive to shallow crustal structure than surface wave group and phase velocity at the same period (Fig. 1) so it is a useful observable, for example, for the characterization of sedimentary basins (e.g. Lin *et al.* 2012). The situation is somewhat similar to that of receiver function studies, in so far teleseismic records can be used to characterise the structure beneath a receiver. Unlike receiver functions, however, ellipticity is

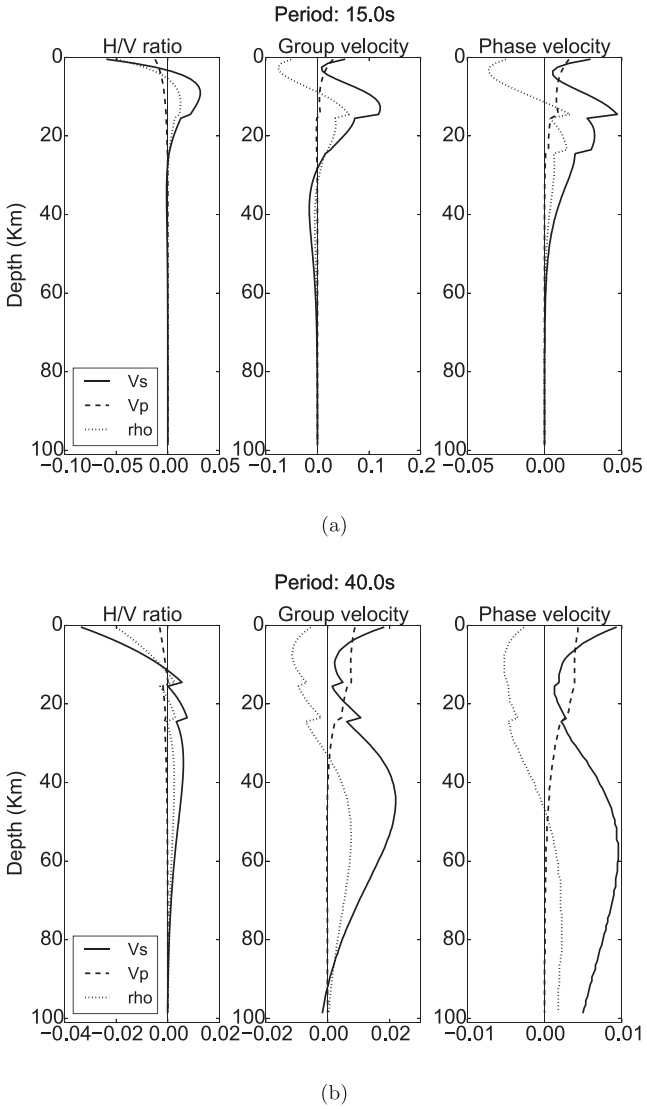

Figure 1. Sensitivity kernels for H/V ratio, group and phase velocity at 15 and 40 s, as a function of v_S (solid line), v_P (dashed line) and density (dotted line) calculated by finite differences using a normal mode formalism for the 1-D PREM global Earth model (Dziewonski & Anderson 1981).

sensitive to seismic velocities (and density) rather than to discontinuities.

The use of Rayleigh wave ellipticity for the determination of crustal structure has been proposed several times in the past (e.g. Boore & Nafi Toksöz 1969) but for decades other seismic observables have been preferred, such as phase and group velocities of surface waves. This was perhaps due to more difficulties in modelling amplitude rather than phase (arrival time) of a seismic pulse. An H/V spectral technique based on ambient noise signals has been introduced by Nogoshi & Igarashi (1971) and Nakamura (1989). This rather empirical technique—that works without proper identification of Rayleigh wave polarization, assuming that background noise is mainly composed by surface waves—has been further developed using small-aperture seismic arrays to derive wavefield characteristics and shear wave velocity profiles (e.g. Di Giulio *et al.* 2006; Wathelet *et al.* 2008), mainly for seismic engineering applications. Over the last decades, a wealth of high-quality seismic data have become available, so the deterministic measurement of ellipticity on the fundamental-mode wave packet of earthquake-generated Rayleigh waves has gained more attention. Some attempts of measuring ellipticity for characterization of deep earth structure have been done by Ferreira & Woodhouse (2007b). They measured ellipticity at the single period of 150 s, and they found substantial variability in amplitude ratios—in contrast with expectations—possibly revealing the presence of small-scale heterogeneity. However, they used a small data set that did not permit a statistical analysis of results. Tanimoto & Rivera (2008) developed two automatic schemes to measure ellipticity on a complete seismogram. They applied the method to all the large events that occurred between 1988 and 2003 recorded by two broad-band stations in Southern California. They showed that by using a very large set of measurements, the results become statistically consistent and in good agreement with theoretical expectations. On the other hand, their study was limited only to two seismic stations. Other studies recently followed this approach, such as Yano *et al.* (2009) and Lin *et al.* (2012, 2014). In particular, Lin *et al.* (2012) jointly inverted H/V measurements together with phase velocities of ambient noise Rayleigh waves in the western United States, using data from all USArray stations available at the time of their study. Phase velocity is sensitive to deeper structure than H/V (Fig. 1) so the joint inversion allows a better illumination of crust and upper-mantle structure. On the other hand, by using phase velocity measurements, the technique is not based on single stations any more.

Northern Italy includes a wide variety of crustal structures ranging from the wide and deep Po Plain sedimentary basin, to outcropping sedimentary and crystalline rocks in the elevated terrains of the Northern Apennines and Alps, representing an excellent laboratory for validating seismic appraisal techniques aimed at gauging shallow earth structure. Tomographically imaged crustal shear wave velocities are generally low beneath the Po Plain and Molasse basins, and high velocities are seen in the crystalline crust of the Alpine mountain belt (e.g. Molinari *et al.* 2015b). This region has been hit in 2012 by two earthquakes, on two close tectonic structures ($M_w = 5.9$ on 2012 May 20 and $M_w = 5.8$ on 2012 May 29) that caused extensive damage, hundreds of injuries and 27 fatalities, in spite of their moderate magnitudes. These events revealed considerable seismic vulnerability of this region, even for relatively modest earthquakes. Significant damage appears to be due to high exposure of this territory associated high density of population and industries, and because of local amplification of seismic waves caused by sedimentary basin structures. Seismic knowledge of this region has recently improved due to renewed interest and recent investigations. For example, the recent 3-D seismic model MAMBo (Molinari *et al.* 2015a) has been constructed collecting and merging information from geological studies and active-source experiments carried on during the 1980s and 1990s decades for hydrocarbon and water research. MAMBo is a rather reliable 3-D model including laterally varying thickness of stratigraphic layers, that has shown to be quite accurate in modelling seismic wave propagation at a regional scale. However, being mostly based on a compilation of geological and geophysical information, MAMBo has not been directly constructed inverting seismic data. The many new broad-band seismic stations deployed in the region in the past decade offer an opportunity to further refine this model. Thus, the northern Italian basin and neighbouring mountain belts, with a large variety of geological terrains, wide availability of recent data, evolving background geological and geophysical studies and a reliable *a priori* seismic model of the crust, seem an excellent candidate for a comprehensive analysis of Rayleigh wave ellipticity.

The main objective of this study is to evaluate the reliability of observation of Rayleigh wave ellipticity, and its dependence on

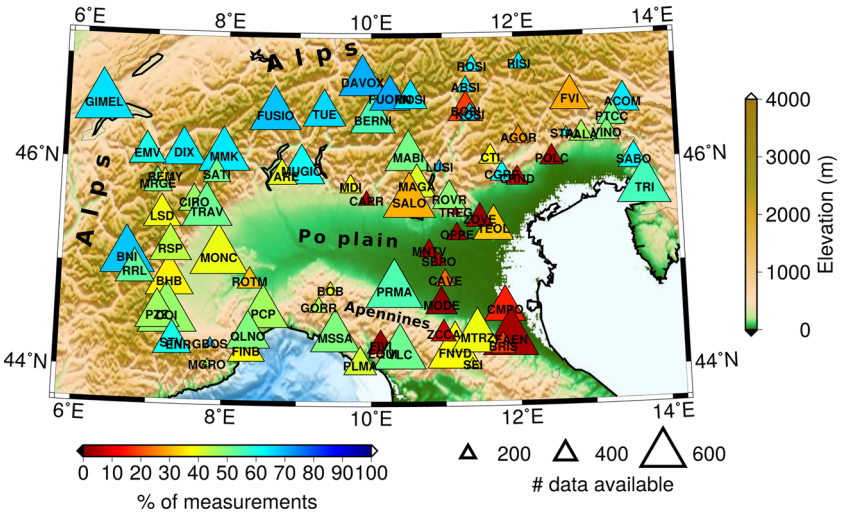

Figure 2. Seismic stations used and corresponding number of measurements. The triangle size indicates the number of earthquake records available for each station and its colour represents the percentage of successful measurements. Stations in the Po Plain sedimentary basin generally perform worse (see the main text).

local crustal structure (or other factors) in diverse geological situations. With this purpose, we carry out extensive measurements on fundamental-mode Rayleigh wave trains from teleseismic earthquake records in Northern Italy. We investigate the reliability and robustness of the measurements, and the response of hard rock *versus* sedimentary sites. We assess potential azimuthal misalignments in the seismic stations in the region, which could have an impact on amplitude measurements. We also quantify the differences between observations and predictions for the MAMBo crustal model, and examine the possibility of identifying prograde *versus* retrograde (normal) particle motion and its use to constrain shallow earth structure. Finally, we assess the validity of our approach using complete theoretical seismograms for a 3-D Earth model.

2 DATA

We focus our attention on the northern part of Italy, in a region encompassing the Po Plain, the northern Apennines and the Alps (Fig. 2). We use data from 95 seismic stations belonging to different networks: Italian Seismic Network (47 stations), South Tyrol Seismic Network (7 stations), North East Italy Broad-Band Network (8 stations), Swiss Seismological Network (9 stations), MEDNET Project (5 stations) and Regional Seismic Network of Northwestern Italy (19 stations). We collected all the data from the ORFEUS Data Center. For each station, we select earthquakes with magnitude $M_w \geq 5.0$ and epicentral distance between 10° and 140° that occurred from 2008 January to 2014 December (a map of events used in this study is shown in Fig. S1 in the Supporting Information). We measure ellipticity on all available data, using the measurement scheme described in the following section, in the period range between 10 and 110 s. We perform measurements excluding all the data with an estimated signal-to-noise ratio (SNR) less than 100. We also remove clear outliers with computed H/V ratio $\geq$10.0 and H/V ratio $\leq$0.1, since such values are not realistic (see theoretical predictions in the next section). We then calculate the median and percentiles of the ellipticity measurements corresponding to $\pm\sigma$.

Fig. 2 shows, for each station, the number of earthquake records retrieved from the database (depending on data availability and station operation), for which an attempt to measure ellipticity has been done, and the success rate, that is, the ratio of number of measurements effectively obtained versus the number of attempts. We note that the measurement success rate is generally much lower for stations in the sedimentary plain than for stations on the mountain belts. This is probably due to two main reasons: (1) noisier locations in the plain, due to anthropic activities and (2) more complex crustal structure of sedimentary layers that causes the superposition of the fundamental mode with overtones, reflected/converted modes and other spurious arrivals. Some of the stations on the plain also have fewer data (smaller triangles in Fig. 2) because they have been installed more recently than other stations.

Measurements of seismic wave amplitudes can be affected by systematic errors due to problems in the station setup, such as orientation or amplitude response of horizontal sensors. If sensor pairs are not perfectly aligned (north and east), the amplitude of the horizontal component of Rayleigh waves will be underestimated, because of the wrong rotation from north and east directions to the radial component of motion. Errors in sensor bearing are not so rare: Ekström & Busby (2008) found alignment errors up to 20° for USArray stations. For this reason, we implemented an algorithm for the determination of possible errors due to the misalignment of sensors. We started from the technique outlined by Ekström & Busby (2008). For each station, we calculate synthetic seismograms using normal mode summation (Gilbert 1970; Herrmann 2013) for PREM (Dziewonski & Anderson 1981) for radial and transverse components, and we compare them to the corresponding components of real data, rotated from N-E (geographical) to R-T (radial-transverse) using the great circle path filtered with a Butterworth-bandpass filter in the range 100–150 s. Then, we rotate the R-T components of real seismograms from −90° to +90° with 1.0° steps. At each step, we compute the correlation coefficient C between the data and the synthetics using the following equation:

$$C = \frac{\sum_{i=1}^{N} o_i s_i}{\sqrt{\sum_{i=1}^{N} o_i^2 \sum_{i=1}^{N} s_i^2}} \quad (1)$$

where o_i are the observed data and s_i are the synthetic. N is the number of time points in the surface wave window. We then recalculate

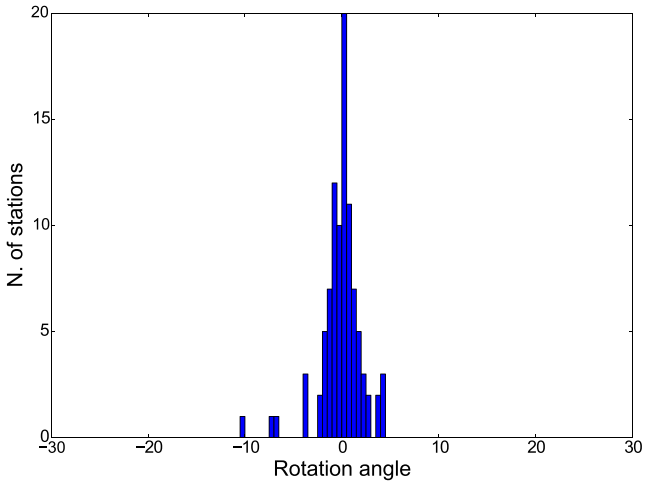

Figure 3. Frequency histogram of azimuthal angle deflections with respect to the theoretical great circle path. The maximum angle found is $\delta\alpha = -10.42^\circ$. Mean $\delta\alpha = -0.07^\circ$. Standard deviation $= 2.15^\circ$.

C for the radial and transverse component at each rotational step. We define the total correlation coefficient C_{TOT} as:

$$C_{\mathrm{TOT}}(\delta\alpha) = \min(|C_R(\delta\alpha)|), |C_T(\delta\alpha)|) \quad (2)$$

where $\delta\alpha$ it the correction angle. The best correction angle $\delta\alpha$ is the one that corresponds to maximum C_{TOT}.

We run the algorithm for each earthquake available and for each station. We statistically summarize the $\delta\alpha$ found and calculate the median for each station. We then obtain a correction angle for each station. The results of this analysis are shown in Fig. 3. We found for most of the stations rather small correction angles: the maximum angle found is -10.42°, but most values are smaller than about 3° (with a mean and standard deviation of -0.07° and 2.15°, respectively), corresponding to a maximum underestimation of the radial amplitude generally less than 0.2 per cent, that is small enough for the purpose of this study. Hence, we do not deem necessary to apply azimuthal corrections for our further analyses.

3 MEASUREMENT SCHEME AND RESULTS

The first and main difficulty in the determination of the H/V ratio are the detection and identification of the Rayleigh fundamental-mode wave train from the rest of the signal. To do this, we look for the particular elliptical and retrograde polarization of Rayleigh waves. In theory, the radial component is 90° phase-advanced with respect to the vertical component for smooth, laterally varying media. Starting from this assumption we implemented a measurement scheme based on that proposed by Tanimoto & Rivera (2008). This is illustrated in Fig. 4.

We first measure the SNR on all the records by comparing the maximum amplitude in the Rayleigh wave time window to the average background noise amplitude in a 10-min pre-event window, and then discard records with SNR below 100. We then apply a narrow Butterworth-bandpass filter to the vertical and radial components, and phase shift the vertical component advancing it by 90°. When the signal consists of fundamental-mode Rayleigh wave motion, the two components will match. We then cross-correlate the radial and the phase-shifted vertical components, and multiply the result by the product of the envelopes of both components. We thus obtain a characteristic function that defines a time window as it exceeds a

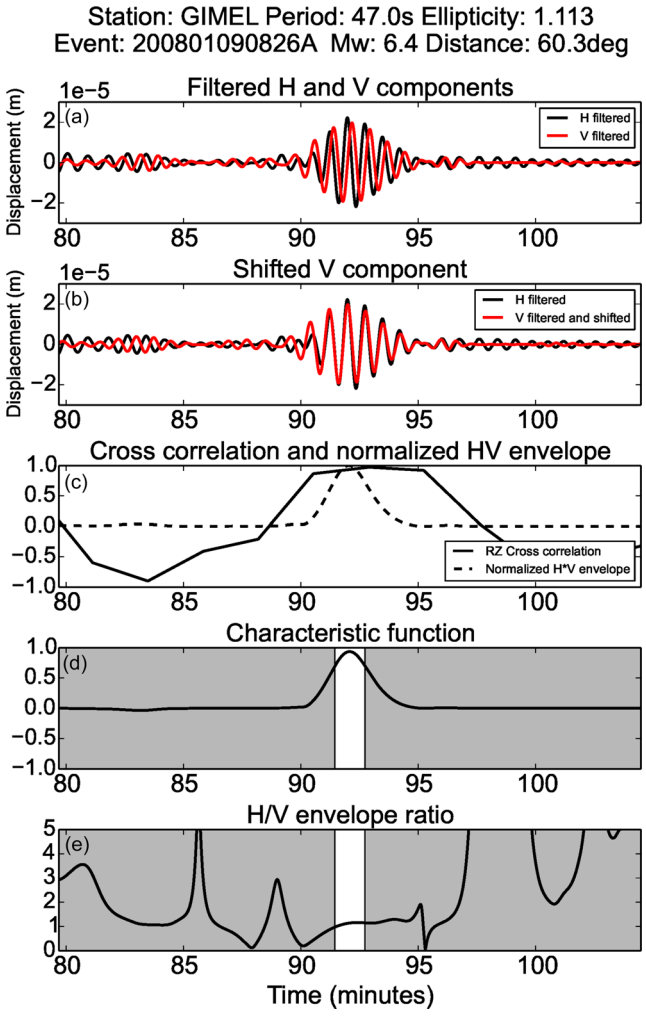

Figure 4. Measurement scheme shown for an earthquake at a distance of 60.3° and magnitude $M_{\mathrm{w}} = 6.4$. (a) We apply a bandpass filter to H and V components and (b) we shift the V component of 90° in advance. Then, (c) we calculate the cross-correlation between the two signals and the envelope. Subsequently, (d) we define a characteristic function as the product of cross-correlation and envelope. This function defines a time window that contains the fundamental mode of Rayleigh waves. (e) We calculate ellipticity as the mean ratio between the V and the H envelope inside the time window.

pre-defined threshold, where the measurement is made. This, in fact, applies a further requirement on the coherence and amplitude of the signal beyond the noise level, as a condition must be met not only on high cross-correlation but also — via multiplication by envelopes — on amplitude of signal as compared to noise. This measurement technique proved very selective, and very effective in separating the fundamental-mode Rayleigh wave from the rest of the signal, but we need a large data set in order to have enough measurements. We carry out these measurements for many earthquakes, and calculate median and percentiles of results. As we consider the ratio of two positive numbers, either of which can become very small, rather than using the straight amplitude ratio—H/V or V/H—we always use and show the logarithm of the ratio $\log_{10}(H/V)$, that is better behaved and statistically more meaningful.

To validate and quantify the ability of this scheme to detect and estimate H/V ratios, we compute synthetic seismograms using normal mode summation and we measure the H/V ratio on these synthetics. We then compare the results with theoretical ellipticity

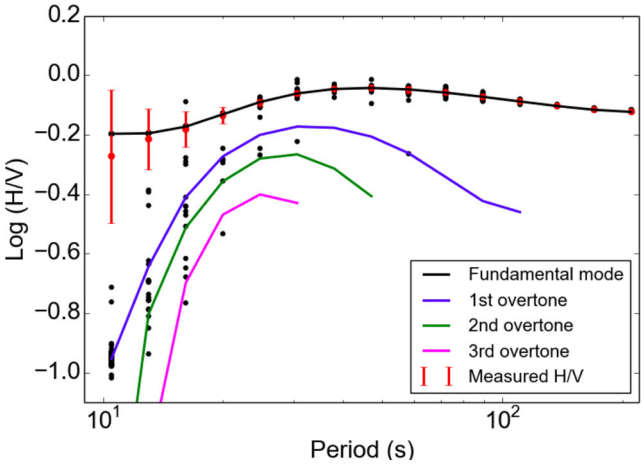

Figure 5. Comparison between theoretical H/V values and measurements on synthetic seismograms, for 426 CMT solutions of real earthquakes. Theoretical ellipticity for the fundamental mode and first three overtones is represented by lines in different colour. Measurements from full synthetic seismograms calculated for PREM correspond to the black dots. Note that there are 426 dots for each period, mostly concentrated near the average, indicated by a red dot with error bars. The presence of overtones (with different ellipticity ratios) influences some measurements at shorter periods, but these appear as outliers well outside the $\pm\sigma$ error bars of the measurements. Note that, for shorter periods, many dots overlap actually appearing as one, near the black curve and control the value of the average shown with error brackets.

curves calculated as the ratio of spheroidal mode horizontal and vertical eigenfunctions evaluated at the Earth surface (e.g. Ferreira & Woodhouse 2007b). For both synthetic seismograms and theoretical values, we use the global model PREM (Dziewonski & Anderson 1981). We perform this calculation for an ensemble of 426 centroid-moment tensors of real earthquakes from the Global CMT catalogue (GCMT, Dziewonski *et al.* 1981; Ekström *et al.* 2012; http://www.globalcmt.org/CMTsearch.html)—the same set used for the analysis on real data. Fig. 5 shows these results, that is, 426 ellipticity values for 15 wave periods between 10 and 200 s. As expected, measured ellipticity mostly concentrates quite well along the theoretical value for the fundamental mode (black line). At shorter periods (<30 s), a few events show a bias of measurements with respect to values expected for the fundamental mode. These outliers can be attributed to the overlap of overtones, which have lower H/V (see Fig. 5) and may in some cases appear conspicuously on the waveforms. In fact, while we did not find any dependence of measured ellipticity on backazimuth, focal mechanism, magnitude, or time, there is some correlation with focal depth, as shown in Fig. 6(a). For focal depths larger than about 40 km the misfit increases. We verify that this is due to the increased excitation of overtones for deeper events. Fig. 6(b) shows the characteristic function, used to identify the wiggles on the seismograms to compute H/V amplitude ratio, for two PREM synthetic seismograms for earthquakes with 20 and 50 km depth. For depths larger than about 40 km, the first overtone dominates and misleads the characteristic function, which affects the ensuing amplitude ratio measurement. In real measurements, a selection of crustal earthquakes therefore avoids this source of error.

We then proceed to make measurements on real data for all the stations shown in Fig. 2, for 12 wave periods between 10 and 110 s. Results for two sample stations are shown in Fig. 7 where, for reference, we also plot the theoretical ellipticity curve for PREM. The behaviour of the measured ellipticity as a function of period is rather smooth and stable. For longer periods, both stations show ellipticity values similar to those of PREM, but deviate quite significantly for the shorter periods. The difference is more notable for PRMA, a station on the edge of the sedimentary basin, than for GIMEL, which is located in the Alps (Fig. 2). This difference reflects different crustal structures beneath the stations, as we will discuss in the following section.

Fig. 8 shows the measured H/V ratios at four sample periods (10, 16, 24 and 37 s) for all stations, superimposed on a map of thickness on the Pliocene sedimentary layer in model MAMBo (Molinari *et al.* 2015a). As explained previously, MAMBo is a recent seismic model of the sedimentary basin of this region, and it integrates information from exploration geophysics and geological studies performed in the last decades for hydrocarbon and water research. It describes the basin with six sedimentary layers, among which the Pliocene deposits represent the seismically most relevant unit. We computed theoretical H/V ratios for this crustal model combined with PREM velocities in the upper mantle. Large-scale tomographic models show only slight lateral variation of shear wave velocity at the top of the mantle over this region, and values always very close (within ±1 per cent) to PREM (e.g. Schivardi & Morelli 2011) so—given the weak sensitivity to mantle depths—this simplification appears legitimate. For each station, such theoretical prediction is shown with colour in the outer ring of symbols in the map of Fig. 8 to be compared with measured values, plotted instead in the inner circle. The Pearson correlation coefficient between predictions and observations is computed for each period, and is shown in the title of each diagram. The measured ellipticity values clearly correlate with geological features. We observe higher values of H/V (reddish colours) for stations in the sedimentary basin (e.g. MNTV, SBPO, CAVE, CMPO, PRMA and ROTM). This is particularly clear for shorter periods (Figs 8a and b), as we expect from the sensitivity kernels (Fig. 1). On the other hand, stations in the Alps and Apennines show lower values of H/V. For the longest wave period (Fig. 8d), we note that stations in the Apennines (southern side of the plain) have higher observed values of H/V compared to Alpine stations, which likely reflects the deeper basement beneath the Apennines than in the Alps (e.g. Molinari *et al.* 2015a).

Comparing the H/V ratio predictions for the MAMBo model (outer rings) and the observations (inner circles), we see that for stations in the Apennines and in the Alps, MAMBo predictions are nearly constant and in good agreement with observations at many stations. However, the observations show some lateral variations not predicted by MAMbo, notably a region of decreased ellipticity in the North Western Alps (Figs 8b and c; e.g. for stations DAVOX, TUE, FUSIO, DIX, MMK, MRGE and LSD). This correlates well with increased upper- and mid-crustal v_P and v_S in the Western Alps, with respect to the Eastern Alps (Gualtieri *et al.* 2014; Molinari *et al.* 2015b) via negative sensitivity of H/V (kernels in Fig. 1). In the Po Plain, the MAMBo model predicts ellipticity values much larger than observed for the two shortest wave periods by a factor of about four (Figs 8a and b); this discrepancy will be discussed in the next section. Finally, there is generally an improved agreement between the predictions and observations for the longest wave period (Fig. 8d), which is probably due to the sensitivity of these data to deeper, simpler structure.

Lateral resolution is still an open issue. The variations also observed at short distances may perhaps be related to the fact that amplitude data are more sensitive to small-scale structure than phase (or traveltimes). Some variability at short spatial scale has indeed been observed in other H/V studies (e.g. Lin *et al.* 2012), but the

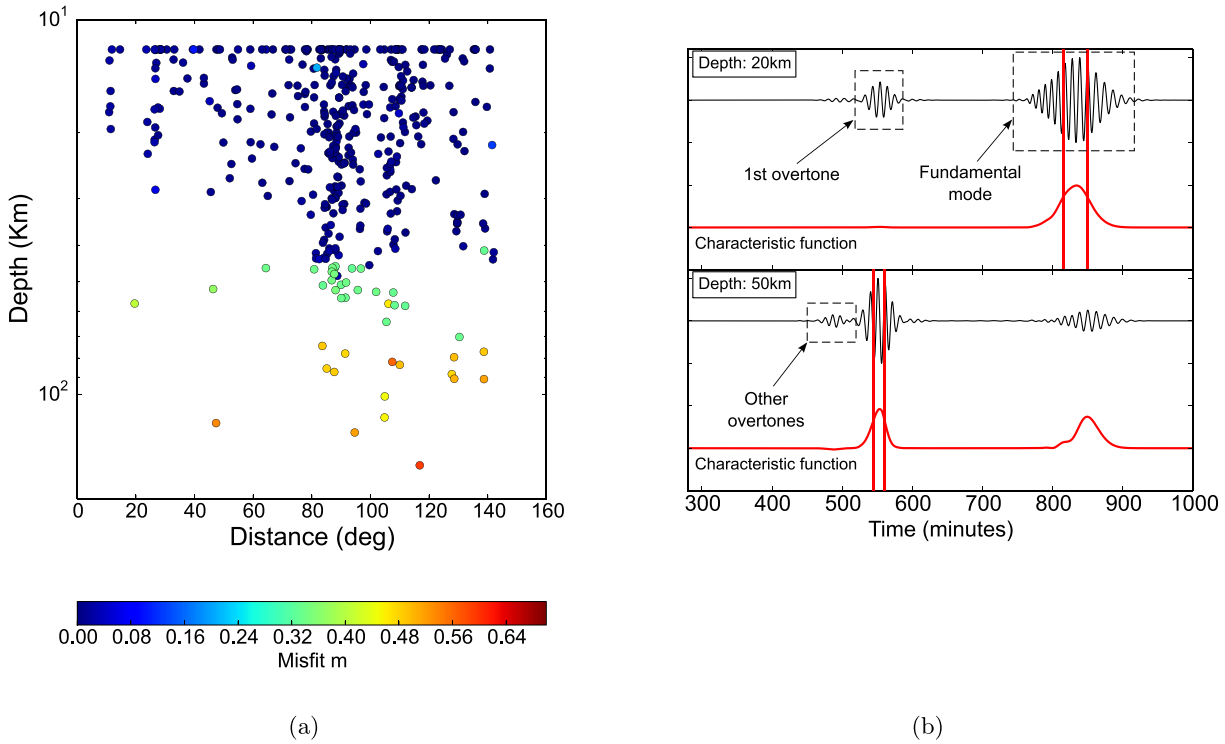

Figure 6. (a) Mean misfit (for all periods) between ellipticity computed for an earthquake on synthetic seismograms and theoretical value, as a function of hypocentral depth. (b) Synthetic seismograms and characteristic function for sample cases for hypocentres at 20 and 50 km depth in PREM. For depths larger than ~ 40 km, the first overtone dominates and misleads the characteristic function. The misfit is calculated using: $m = \frac{\sum_{i=1}^{N} |E_i^m - E_i^t|}{\sum_{i=1}^{N} |E_i^m|}$, where N is the number of periods, E^m is the ellipticity measured on synthetics and E^t is the theoretical ellipticity calculated from eigenfunctions.

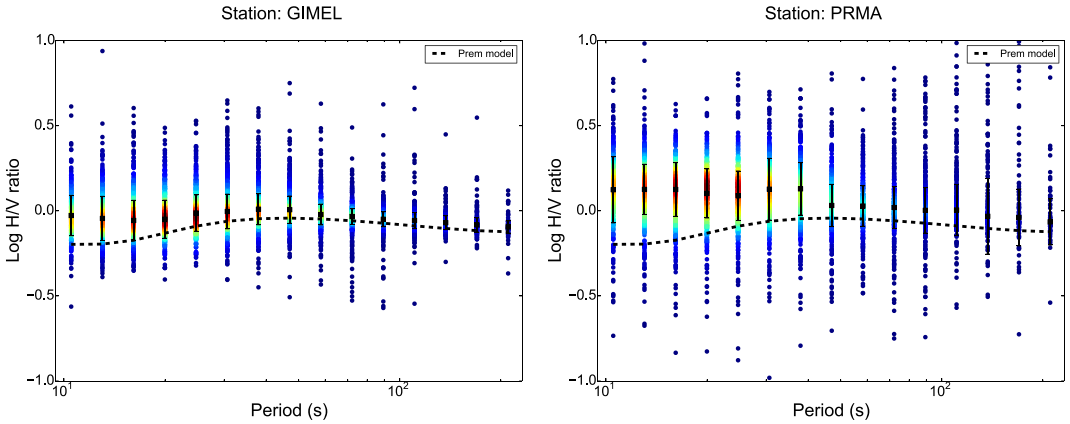

Figure 7. H/V measurements for stations GIMEL and PRMA as a function of period. Different colours show the density of dots. Dashed line is the theoretical ellipticity for the PREM model.

larger spacing between USArray stations used (about 70 km) does not allow a clear assessment. The SEM simulations we show here (see Section 4) are not very informative to this purpose, because the crustal model we use has resolution wider than the station spacing, and hence not very relevant for this particular test. Unfortunately computing synthetics with such a fine grid needs longer computational time and would be well beyond the scope of this study. We may also speculate that, because sensitivity kernels are shallow and very peaked at the surface, a local, very shallow, very slow heterogeneity could in principle affect one single station only and not show up in neighbouring ones, even for the longer of the periods we consider.

4 RAYLEIGH WAVE ELLIPTICITY PREDICTIONS FROM 3-D SYNTHETICS

Ellipticity of Rayleigh waves is a local property of the elastic medium. In this, it is not different from, for example, phase velocity. However, generally we cannot measure local phase velocity directly: rather, we measure a phase difference (or a traveltime) between two points at some distance, so a phase measurement brings information on phase velocity integrated along a path. Measurement of ellipticity at a single station, instead, brings information solely on the structure beneath the seismograph, and not about the whole path travelled by the wave. This dependency of ellipticity only on the structure beneath the receiver station can be demonstrated for a

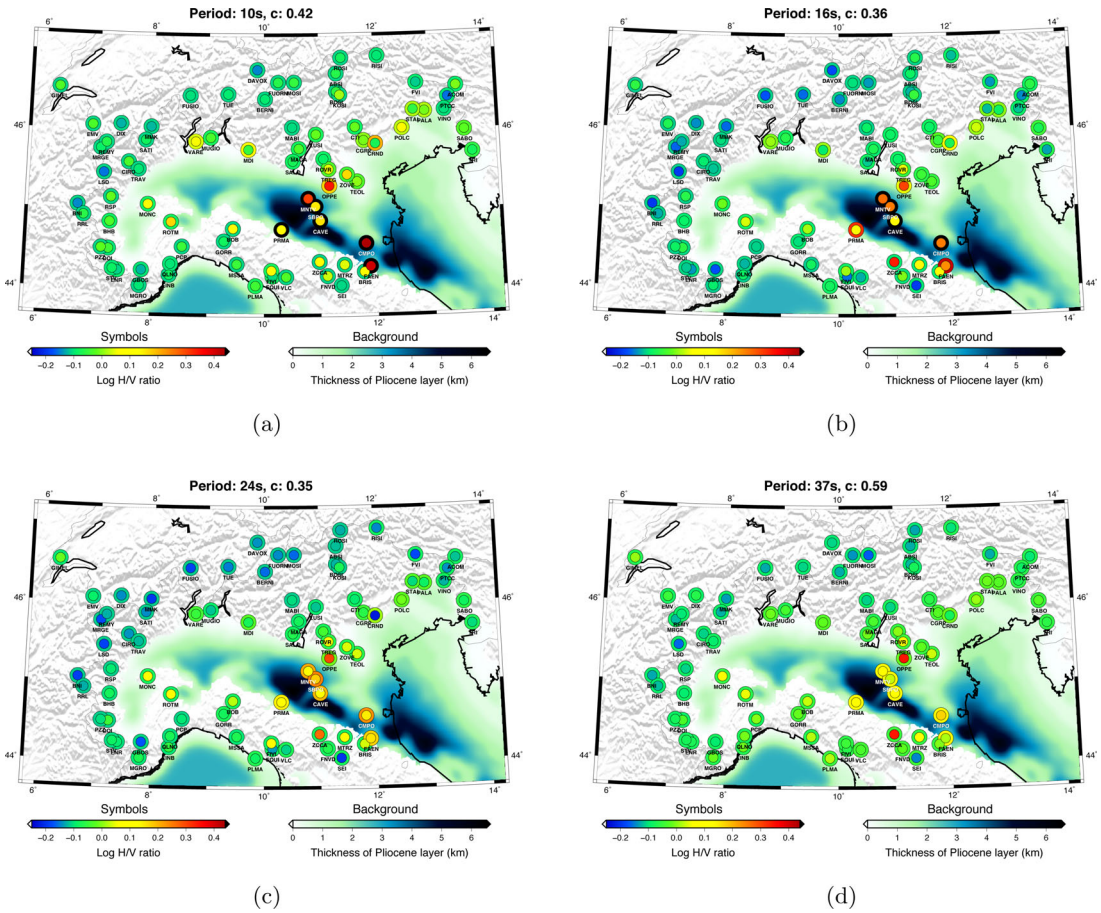

Figure 8. H/V ratios for different periods (shown in coloured solid circles) compared with theoretical values for model MAMBo (Molinari *et al.* 2015a) shown in the outer rings. Black outer ring means that ellipticity values are greater than 0.6, going up to 2.0 (FAEN station). The Pearson correlation coefficient between the observations and predictions is shown in the title of each diagram. The background shows thickness of the Pliocene sedimentary layer according to model MAMBo.

smooth, laterally heterogeneous, slightly anisotropic, anelastic, non-rotating, self-gravitating medium using full ray theory (e.g. Ferreira & Woodhouse 2007a,b). However, one can question whether such description is valid for realistic 3-D Earth models and for the wave periods considered in this study.

In order to address this question, we perform a synthetic test. We compute synthetic seismograms of a real earthquake with `SPECFEM3D_GLOBE` (Komatitsch & Tromp 2002; Peter *et al.* 2011), which is a widely used code for the simulation of seismic wave propagation. It is based on the spectral-element method (SEM) and it accurately simulates complete waveforms in complex media. We perform simulations using a global 3-D Earth model combining the recent global mantle model SGLOBE-rani (Chang *et al.* 2015) with the crustal model Crust2.0 (Bassin *et al.* 2000). We use an event that occurred in Costa Rica on 2012 July 5, with $M_w = 6.8$ and 29.7 km hypocentral depth, at a distance of approximately 88° from the area of study. The SEM synthetics are computed using 3456 processors and are accurate down to a period of ~ 5.6 s. H/V ratios are then measured on the SEM synthetics using the same measurement technique as that used with real data. We also compute theoretical ellipticity using 1-D models with the same structure as in the 3-D Earth model beneath each station in Northern Italy. We then compare the SEM H/V ratios with the theoretical predictions from the 1-D models as a function of the wave period. We see in Fig. 9 that overall there is a good agreement between the values of ellipticity measured on the 3-D synthetics and the theoretical predictions for the local 1-D models, notably for wave period $T \sim$ 25–72 s. Differences are always smaller than the errors of real data measurements shown as grey error bars, which further strengthens the validity of our approach. We also compare the SEM H/V ratios with real data measurements (Fig. 10). As expected, there are larger differences between them than in Fig. 9 because the real structure in the study region is much more complex than in CRUST2.0. These discrepancies, along with the differences between predictions and observations seen in Fig. 8, highlight that inversions of the observed H/V ratios for elastic structure as a function of depth should help refine Earth structure models of the study region. Nevertheless, it is important to bear in mind that these comparisons are only for one earthquake (due to the high computational cost of the SEM simulations accurate down to $T \sim 5.6$ s). Hence, probably part of the differences observed in these tests are mitigated by the fact that in real data applications a very large number of events along with strict data selection criteria are used to ensure stable measurements of H/V ratios.

5 PROGRADE RAYLEIGH WAVE MOTION

Rayleigh wave elliptical polarization usually implies retrograde particle motion at the surface, but inverts polarity and becomes prograde at a certain depth. This behaviour can be seen theoretically for

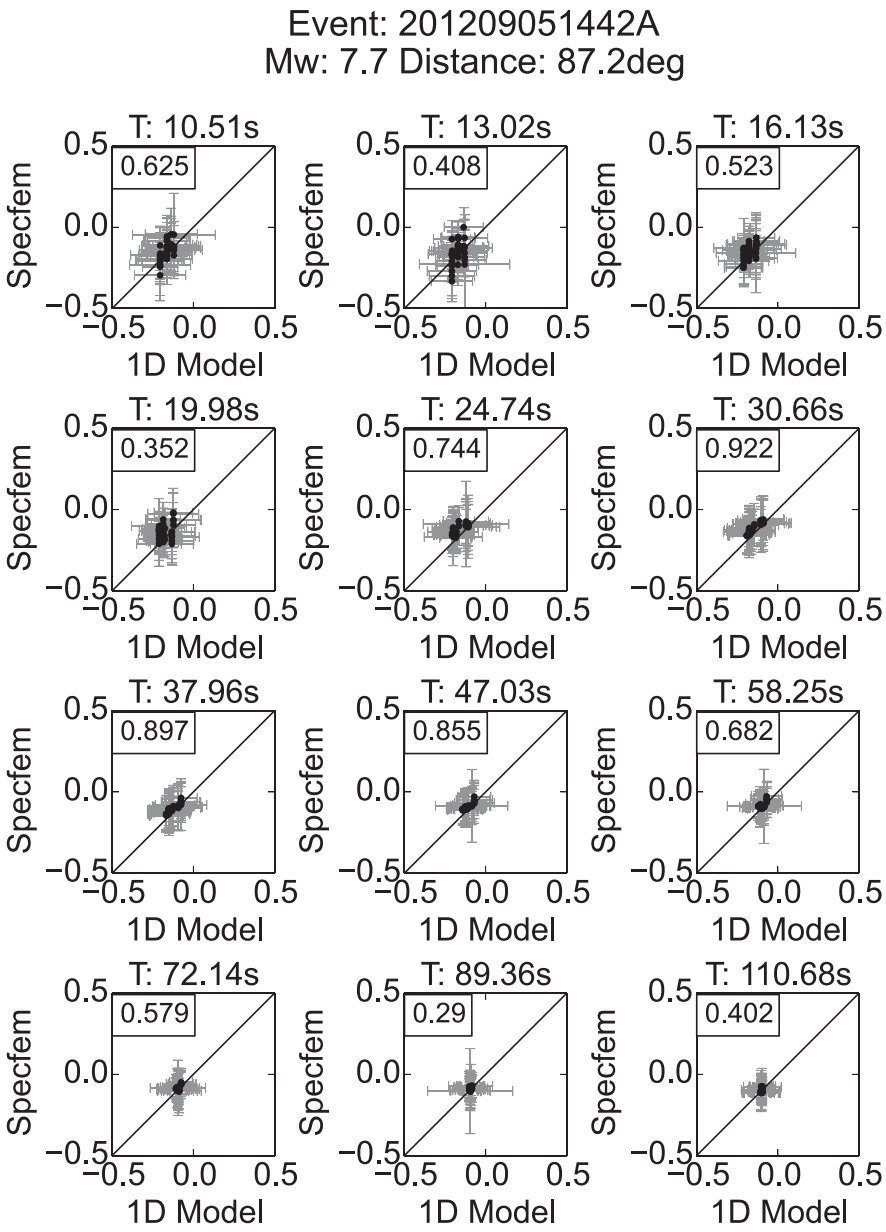

Figure 9. Comparison between ellipticity measured on synthetics seismograms computed with a 3-D model and ellipticity measured on synthetics computed with a 1-D model built using the 3-D profiles beneath each station. The bars are the errors associated with real measurements from each station. They give an estimate of the errors expected in real measurements (see Fig. 10). In the boxes, the correlation coefficient between the two data sets is shown. This test shows that the local 1-D approximation at the receiver can be used instead of a 3-D model from source to receiver. The errors are always under the observed data errors.

Rayleigh waves in a homogeneous half-space (e.g. Stein & Wysession 2003). However, in some cases, it may happen that the Rayleigh wave fundamental mode shows prograde particle motion at the surface, for example, when a very slow sedimentary layer is overlaid onto a faster crustal structure. Tanimoto & Rivera (2005) studied this phenomenon with numerical simulations using a mode summation technique, and showed that such sign inversion of the elliptically polarised motion of Rayleigh waves may indeed take place near the surface in the period range 3.8–7.1 s for a sedimentary layer of 4 km. They also found a correlation between the thickness of the sedimentary layer and the period where the reversal begins: the thicker is the layer, the longer the inversion period is. No inversion has been found if the sedimentary layer is thinner than 2 km.

Since, on sedimentary basins, Rayleigh wave particle motion trajectories may transition to prograde polarity, we could potentially face measurement instabilities near the period corresponding to the transition from ‘normal’ (retrograde) to prograde motion in Po Plain stations. In order to investigate this issue, we compare theoretical ellipticity curves from the MAMBo model for stations in the Po Plain with values measured on synthetic seismograms computed by normal mode summation for the same model. In order to allow prograde motion to be detected, we modify our measurement algorithm to allow separation of retrograde from prograde motion, by considering for simplicity that prograde motion would show a cross-correlation equal to -1 (rather than $+1$), maintaining the usual (positive) phase shift.

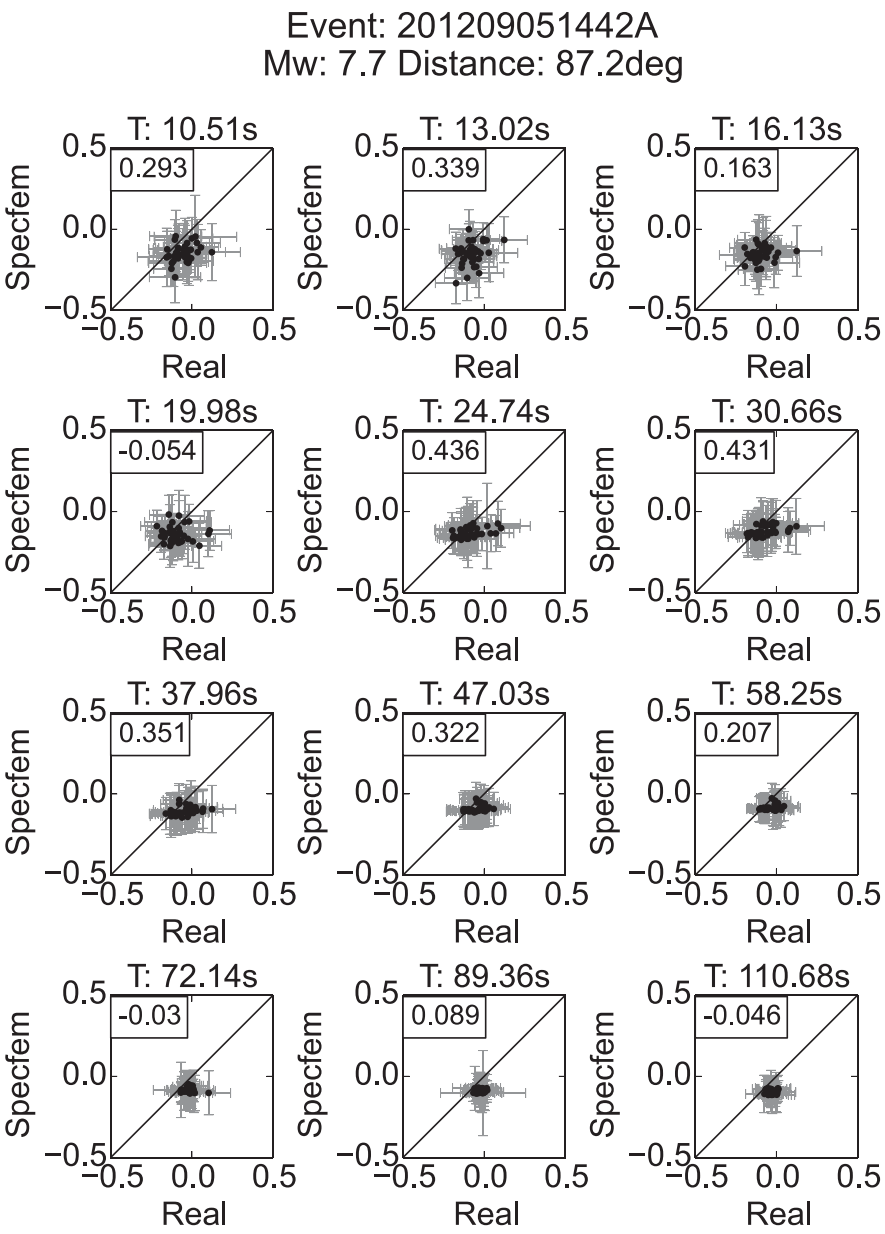

Figure 10. Comparison between ellipticity of synthetic seismogram computed with 3-D model and real data. *x* and *y* error bars are from real measurements. In the boxes, there is the correlation coefficient.

Fig. 11 presents the results of measurements on the mode summation synthetics for station CMPO. We note a big peak in the theoretical curve at a period of about 12.5 s corresponding to the transition period between retrograde motion (on the right) and prograde motion (on the left). This also explains the very large predicted ellipticity values in the Po Plain seen in Figs 8(a) and (b). Measurements performed on the synthetics align along the theoretical curve, except for the amplitude of the transition peak, which corresponds to a singularity, and hence where the bigger mismatch occurs. Nevertheless, the overall behaviour of the theoretical curve is captured well, and gives us some clues on the expected behaviour for real data measurements.

We then calculate the theoretical transition period for the whole study area as expected by the MAMBo model, and shown results in Fig. 12. The transition period is longer for stations on the plain than elsewhere, and no inversion from retrograde to prograde motion is predicted for periods $T > 1$ s for stations on hard-rock sites on the mountain chains, where the motion is always expected to be retrograde.

Fig. 12 shows that the expected transition periods are in the range 2–16 s with longer periods in the southern part of the plain, in a region parallel to the Apennines chain (around PRMA, CMPO, CAVE and MODE stations). In this area, the sediments reach a thickness of 6–8 km (Molinari *et al.* 2015a). In such a geological setting, the expected inversion periods of 10–13 s are compatible with the values predicted by Tanimoto & Rivera (2005) for the Los Angeles basin, that has similar geological features, where they predicted the transition in the period range between 3 and 20 s.

Finally, we measure ellipticity on real data for all the stations in the Po Plain separating retrograde from prograde motion in the same way as in the synthetic test explained above. For comparison, we also carry out the same analysis for station BNI in the Western Alps. Fig. 13 compares histograms of the results for stations BNI and CMPO, the latter being located in the Po Plain (the results for

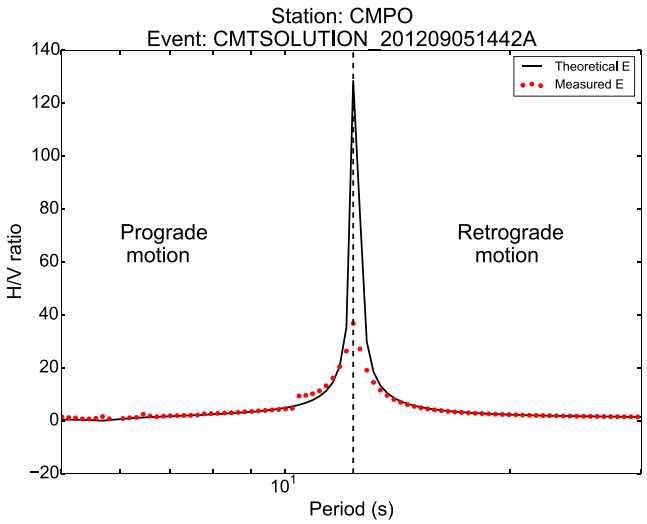

Figure 11. Theoretical ellipticity curve (solid black line) compared to ellipticity measured on synthetic seismogram (red dots) computed for model MAMBo at station CMPO (for location, see Fig. 2). The big peak at ∼12.5 s corresponds to the transition between retrograde motion (on the right) and prograde motion (on the left).

the other stations in the Plain are similar to CMPO). Fig. 13 shows that at CMPO for periods shorter than 13.3 s, the detections of prograde motion on earthquake seismograms generally increase as the period decreases, where they are mixed with retrograde motion. This suggests that there may be an actual transition period around ∼13.0 s, from which both prograde and retrograde motion can sometimes be detected. This agrees well with the transition period predicted by MAMBo (Fig. 11). On the other hand, for station BNI there seems to be no transition to prograde motion down to 10 s. In both cases, it is difficult to measure ellipticity for shorter periods on earthquake data, because of the surge of microseismic noise where prograde and retrograde detections are mixed together (possible coherent noise wave trains may come from all azimuths, hence they present complete ambiguity on motion polarity). Moreover, the presence of ambient noise propagating in the same or opposite azimuth of the earthquake may also lead to detections of signals in the vertical component, which may reduce the measured H/V ratios. Hence, while these results suggest that for station CMPO we may have detected a transition period around 13 s, further work based on analysis of azimuthal distribution and polarization of ambient noise signal is needed for firmer conclusions. For time-domain waveforms recorded at station CMPO, see Figs S3 and S4 in the Supporting Information.

6 DISCUSSION AND CONCLUSIONS

We measured ellipticity H/V of Rayleigh waves in Northern Italy in the period range 10–110 s using an automatic scheme that showed good capability of detection and separation of fundamental mode of Rayleigh waves from the rest of the signal. A large volume of high-quality teleseismic recordings in 2008–2014 has been used and we investigated potential horizontal component misalignments in the seismic stations used, which were found to be negligible.

Rayleigh wave ellipticity is sensitive to shallower structure than phase and group velocity for the same period. It is mostly sensitive to v_S, but it is also sensitive to v_P and density. However, the dependence of ellipticity on earth structure is more complex than that of phase or group velocity, because sensitivity kernels change sign with depth. Sensitivity to v_S is typically negative near the surface and becomes positive deeper in the crust, with a zero-crossing at some depth that depends on the wave period (Fig. 1). Hence, a shallow fast v_S anomaly generates a low ellipticity value, whereas the same fast anomaly at greater depths leads to a high ellipticity value.

Our new measurements of H/V ratios show a good spatial coherence and excellent correlation with geological features, and exhibit small-scale variations, possibly highlighting small-scale heterogeneity. Locations of high ellipticity correspond to regions of low velocity in the Po plain sedimentary basin. Conversely, seismically faster hard rock regions in the Alps and Apennine mountain ranges show lower ellipticity values. Moreover, the observed ellipticity values also relate to the thickness of the basement, as highlighted by differences in observations beneath the Alps and the Apennines, notably for wave periods of $T \sim 37$ s.

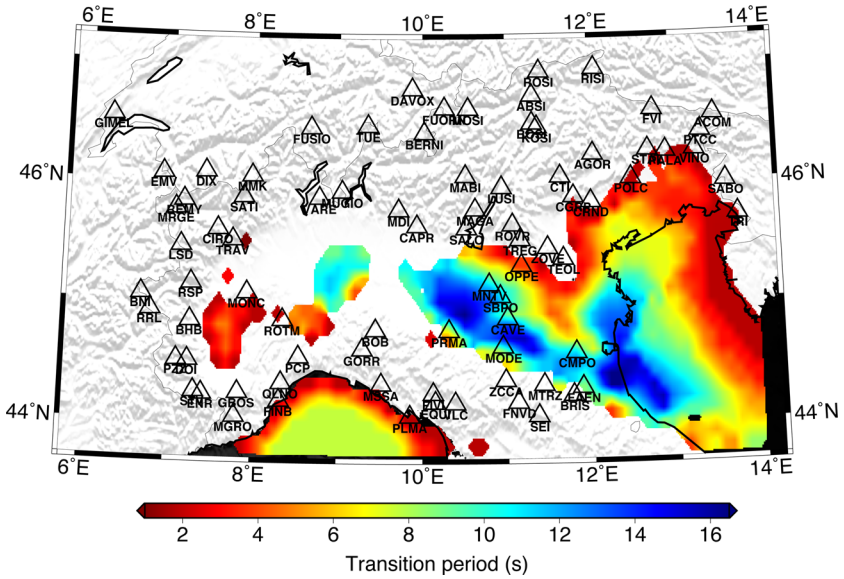

Figure 12. Map of the transition period between retrograde and prograde particle motion calculated on model MAMBo. In blank areas, no transition is found for $T > 1$ s.

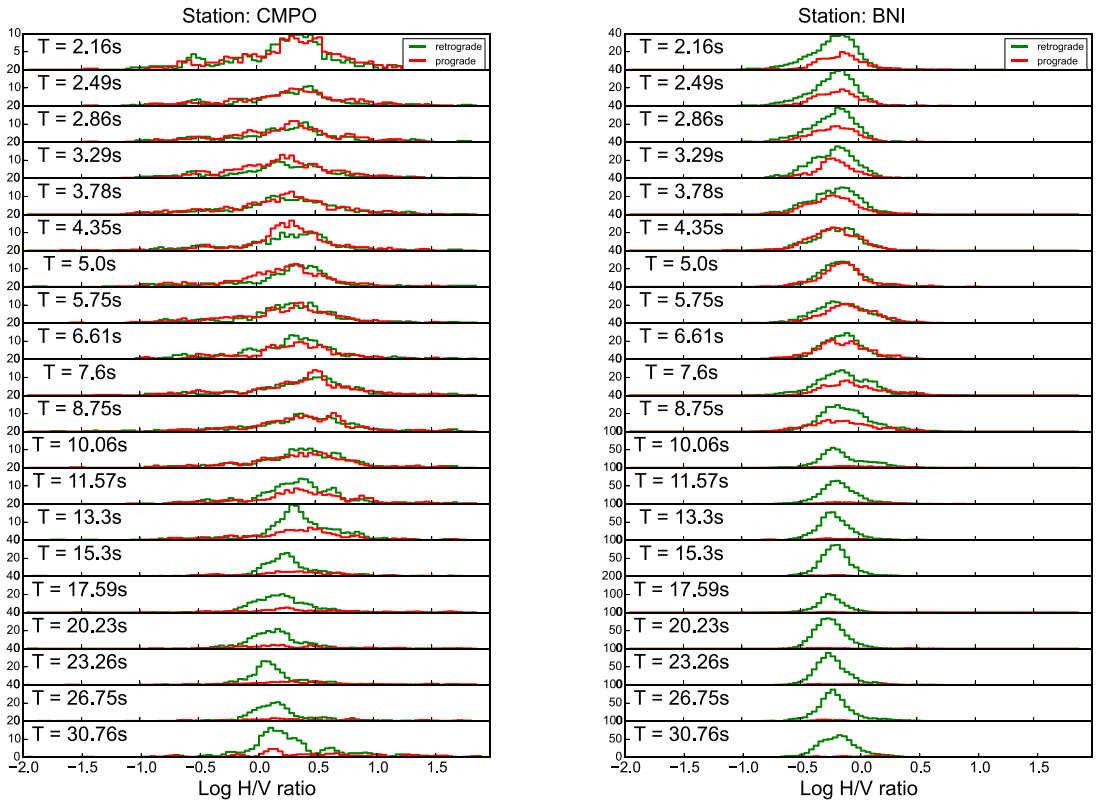

(a) (b)

Figure 13. Histograms of ellipticity measurements for station (a) CMPO and (b) BNI. Green histograms represent the measurements of retrograde particle motion. Red histograms represents the measurements of prograde motion.

Comparisons between observations and predicted H/V ratios for the MAMBo model show a reasonable agreement in terms of the first-order patterns, particularly for the longest period data ($T \sim$ 37 s). For the two shortest wave periods considered ($T \sim$ 10 and 16 s), the predictions for the Po Plain are larger than the observations by a factor of four or more. This is due to the fact that for $T \sim$ 10–13 s MAMBo predicts an inversion from retrograde to prograde Rayleigh wave particle motion at the surface in the Plain, where the vanishing amplitude of vertical component of motion leads to a singularity in the ellipticity, and hence to very large predicted values. Analysis of real data from the Plain allowing the detection of both retrograde and prograde surface wave particle motions suggests possible detection of prograde particle motion. However, the mix of weak teleseismic earthquake signals with ambient noise at the predicted transition periods complicates the interpretation of the results. Future work should be carried out analysing the polarization and ellipticity of both earthquake and ambient noise data, including azimuthal analyses, which are beyond the scope of this study. Nevertheless, when robust detections of inversion periods are confirmed, they could provide key information about the structure of sedimentary basins, notably about their thickness.

In order to test whether ellipticity depends only on the structure beneath the receiver station for realistic 3-D Earth models, we use our technique to compute Rayleigh ellipticity using accurate theoretical seismograms calculated using the SEM for a recent 3-D mantle model and a global crustal 3-D Earth model. Our results show an overall good agreement between the measurements on the 3-D synthetics and the ray theory, local receiver structure predictions, within the measurement errors. These tests help us further validate our technique. A significant step of the Moho under the Northern Apennines has been shown to reflect laterally surface waves in the 15–20 s period band (Stich & Morelli 2007) and has been imaged from time reversal of reflected surface waves along the axial zone of the mountain chain (Stich *et al.* 2009). Such a strong and sharp lateral gradient of structure could possibly perturb ellipticity measurements, but we find no clear indication of that in our measurements. However, actual sensitivity of elliptical polarization parameters in situations far from a flat layered medium, or its smooth perturbations, still have to be explored in detail.

Besides an overall fair agreement between theoretically predicted and observed values, we also image geographically coherent deviations from expectations. This makes us conclude that ellipticity may indeed represent an appropriate tool for improving knowledge of shallow crustal structure. The strong non-linearity of its dependence, represented by highly variable sensitivity kernels, may grant resolution, but makes the inversion more complex. Joint inversion with other observables—such as surface wave group and phase velocities, or body wave receiver functions—may result beneficial to this extent.

ACKNOWLEDGEMENTS

Data used in this study were collected from ORFEUS-EIDA Data Center and they have been provided by several networks: Italian National Seismic Network operated by Istituto Nazionale di Geofisica e Vulcanologia (http://eida.rm.ingv.it/): 47 stations. Province Südtirol seismic network operated by ZAMG—Central Institute for Meteorology and Geodynamics: 7 stations. North-East Italy Broad-band

Network (OGS and University of Trieste 2002): 8 stations. Switzerland Seismological Network (http://www.seismo.ethz.ch/): 9 stations. MedNet Project (http://mednet.rm.ingv.it): 5 stations. Regional Seismic Network of North Western Italy (University of Genova 1967): 19 stations.

Data analysis and measurements have been performed using ObsPy (Beyreuther *et al.* 2010; Megies *et al.* 2011; Krischer *et al.* 2015). AMGF thanks funding by the Fundacao para a Ciencia e Tecnologia (FCT) project AQUAREL (PTDC/CTE-GIX/116819/2010) and computing time in the UK supercomputer Archer. AMGF is also grateful for funding from NERC project NE/K005669/1.

REFERENCES

Bassin, C., Laske, G. & Masters, G., 2000. The current limits of resolution for surface wave tomography in North America, *EOS, Trans. Am. geophys. Un.,* **81,** F897.

Beyreuther, M., Barsch, R., Krischer, L., Megies, T., Behr, Y. & Wassermann, J., 2010. ObsPy: a python toolbox for seismology, *Seismol. Res. Lett.,* **81**(3), 530–533.

Boore, D. & Nafi Toksöz, M., 1969. Rayleigh wave particle motion and crustal structure, *Bull. seism. Soc. Am.,* **59,** 331–346.

Chang, S.-J., Ferreira, A.M.G., Ritsema, J., van Heijst, H.J. & Woodhouse, J.H., 2015. Joint inversion for global isotropic and radially anisotropic mantle structure including crustal thickness perturbations, *J. geophys. Res.,* **120**(6), 4278–4300.

Dziewonski, A.M. & Anderson, D.L., 1981. Preliminary reference Earth model, *Phys. Earth planet. Inter.,* **25**(4), 297–356.

Dziewonski, A.M., Chou, T.A. & Woodhouse, J.H., 1981. Determination of earthquake source parameters from waveform data for studies of global and regional seismicity, *J. geophys. Res.,* **86**(B4), 2825–2852.

Di Giulio, G., Cornou, C., Ohrnberger, M., Wathelet, M. & Rovelli, A., 2006. Deriving wavefield characteristics and shear-velocity profiles from two-dimensional small-aperture arrays analysis of ambient vibrations in a small-size alluvial basin, Colfiorito, Italy, *Bull. seism. Soc. Am.,* **96,** 1915–1933.

Ekström, G. & Busby, R.W., 2008. Measurements of seismic orientation at USArray transportable array and backbone stations, *Seismol. Res. Lett.,* **79**(4), 554–561.

Ekström, G., Nettles, M. & Dziewonski, A.M., 2012. The global CMT Project 2004–2010: centroid-moment tensors for 13,017 earthquakes, *Phys. Earth planet. Inter.,* **200–201,** 1–9.

Ferreira, A.M.G. & Woodhouse, J.H., 2007a. Source, path and receiver effects on seismic surface waves, *Geophys. J. Int.,* **168,** 109–132.

Ferreira, A.M.G. & Woodhouse, J.H., 2007b. Observations of long period Rayleigh wave ellipticity, *Geophys. J. Int.,* **169,** 161–169.

Gilbert, F., 1970. Excitation of normal modes of the earth by earthquake sources, *Geophys. J. R. astr. Soc.,* **22,** 223–226.

Gualtieri, L., Serretti, P. & Morelli, A., 2014. Finite-difference P-wave travel time seismic tomography of the crust and uppermost mantle in the Italian region, *Geochem. Geophys. Geosyst.,* **15,** 69–88.

Herrmann, R.B., 2013. Computer programs in seismology: an evolving tool for instruction and research, *Seismol. Res. Lett.,* **84**(6), 1081–1088.

Komatitsch, D. & Tromp, J., 2002. Spectral-element simulations of global seismic wave propagation: I. Validation, *Geophys. J. Int.,* **149** 390–412.

Krischer, L., Megies, T., Barsch, R., Beyreuther, M., Lecocq, T., Caudron, C. & Wassermann, J., 2015. ObsPy: a bridge for seismology into the scientific Python ecosystem, *Comput. Sci. Discovery,* **8**(1), 014003, doi:10.1088/1749-4699/8/1/014003.

Lin, F.-C., Schmandt, B. & Tsai, V.C., 2012. Joint inversion of Rayleigh wave phase velocity and ellipticity using USArray: constraining velocity and density structure in the upper crust, *Geophys. Res. Lett.,* **39,** L12303, doi:10.1029/2012GL052196.

Lin, F.-C., Tsai, V.C. & Schmandt, B., 2014. 3-D crustal structure of the western United States: application of Rayleigh-wave ellipticity extracted from noise cross-correlations, *Geophys. J. Int.,* **198**(2), 656–670.

Megies, T., Beyreuther, M., Barsch, R., Krischer, L. & Wassermann, J., 2011. ObsPy—what can it do for data centers and observatories?, *Ann. Geophys.,* **54**(1), 47–58.

Molinari, I., Argnani, A., Morelli, A. & Basini, P., 2015a. Development and testing of a 3D seismic 2 velocity model of the Po Plain sedimentary basin, Italy, *Bull. seism. Soc. Am.,* **105**(2a), doi:10.1785/0120140204.

Molinari, I., Verbeke, J., Boschi, L., Kissling, E. & Morelli, A., 2015b. Italian and Alpine three-dimensional crustal structure imaged by ambient-noise surface-wave dispersion, *Geochem. Geophys. Geosyst.,* **16,** doi:10.1002/2015GC006176.

Nakamura, Y., 1989. A method for dynamic characteristics estimation of subsurface using microtremor on the ground surface, *Q. Rep. Railw. Tech. Res. Inst.,* **30**(1), 25–30.

Nogoshi, M. & Igarashi, T., 1971. On the amplitude characteristics of microtremor (Part 2) (in Japanese with english abstract), *J. Seismol. Soc. Japan,* **24,** 26–40.

OGS (Istituto Nazionale di Oceanografia e di Geofisica Sperimentale) and University of Trieste, 2002. *North-East Italy Broadband Network,* International Federation of Digital Seismograph Networks. Other/Seismic Network, doi:10.7914/SN/NI.

Peter, D. *et al.*, 2011. Forward and adjoint simulations of seismic wave propagation on fully unstructured hexahedral meshes, *Geophys. J. Int.,* **186,** 712–739.

Schivardi, R. & Morelli, A., 2011, EPmantle: a three-dimensional transversely isotropic model of the upper mantle under the European Plate, *Geophys. J. Int.,* **185,** 469–484.

Stein, S. & Wysession, M.E., 2003. *An Introduction to Seismology, Earthquakes, and Earth Structure*, Wiley Blackwell.

Stich, D. & Morelli, A., 2007. Reflection of seismic surface waves at the northern Apennines, *Earth planet. Sci. Lett.,* **259,** 149, doi:10.1016/j.epsl.2007.04.036.

Stich, D., Danecek, P., Morelli, A. & Tromp, J., 2009. Imaging lateral heterogeneity in the northern Apennines from time reversal of reflected surface waves, *Geophys. J. Int.,* **177,** 543–554.

Tanimoto, T. & Rivera, L., 2005. Prograde Rayleigh wave particle motion, *Geophys. J. Int.,* **162,** 399–405.

Tanimoto, T. & Rivera, L., 2008. The ZH ratio method for long-period seismic data: sensitivity kernels and observational techniques, *Geophys. J. Int.,* **172,** 187–198.

University of Genova, 1967. *Regional Seismic Network of North Western Italy,* International Federation of Digital Seismograph Networks. Other/Seismic Network, doi:10.7914/SN/GU.

Wathelet, M., Jongmans, D., Ohrnberger, M. & Bonnefoy-Claudet, S., 2008. Array performances for ambient vibrations on a shallow structure and consequences over V_S inversion, *J. Seismol.,* **12,** 1–19.

Woodhouse, J.H., 1974. Surface waves in a laterally varying layered structure, *Geophys. J. R. astr. Soc.,* **37,** 461–490.

Yano, T., Tanimoto, T. & Rivera, L., 2009. The ZH ratio method for long-period seismic data: inversion for S-wave velocity structure, *Geophys. J. Int.,* **179,** 413–424.

SUPPORTING INFORMATION

Additional Supporting Information may be found in the online version of this paper:

Figure S1: Distribution of the events database used in this study. We used earthquake with epicentral distance between 10° and 140° from the stations and mw ≥ 5.0 occurred from January 2008 to December 2014.

Figure S2: Histograms of ellipticity measurements for station GIMEL (a) and PRMA (b). Red vertical line indicates *H/V* median, also reported in the labels with the corresponding error. Errors are calculated using the percentiles corresponding to 15.9 and 84.1.

Green dashed line is the ellipticity calculated on Prem reference model.

Figure S3: Measurement scheme for the March 11 2011 earthquake in the Tohoku region (Japan) (origin time: 05:46:23.00 UTC, mw = 9.0) recorded at the station CMPO at a period of 4 s (left) and 8 s (right). (a) Full waveforms filtered with a narrow Butterworth-Bandpass filter. Vertical component is plotted in red, horizontal (radial) component is plotted in black. (b) Zoom of the waveform. The phase ov the vertical component has been advanced by 90 deg, as expected for 'normal' polarity, i.e. retrograde elliptical particle motion. Horizontal and vertical components result here anti-correlated. (c) Cross-correlation between the de-phased vertical component and horizontal component (solid line) and normalized envelope of horizontal times vertical components. Negative cross-correlation indicates a prograde polarization of Raileigh waves. (d) Characteristic function, defined as the product of envelope and cross-correlation. (e) *H/V* ratio between the envelopes of horizontal and vertical component.

Figure S4: Same as in Fig. S3, but for signal filtered at longer periods (12 s and 16 s). At these frequencies, the same phase shift brings the horizontal and vertical components in phase, and cross-correlation is positive, as expected for 'normal', retrograde-motion polarization.

(http://gji.oxfordjournals.org/lookup/suppl/doi:10.1093/gji/ggw159/-/DC1).

Please note: Oxford University Press is not responsible for the content or functionality of any supporting materials supplied by the authors. Any queries (other than missing material) should be directed to the corresponding author for the paper.